Pergamon

Int. J. Heat Mass Transfer. Vol. 40, No. 5, pp. 1071–1081, 1997

0017–9310/97 $17.00 + 0.00

PII: S0017-9310(96)00159-7

Heat transfer and flow field in a pipe with sinusoidal wavy surface—II. Experimental investigation

G. RUSS and H. BEER

Institut für Technische Thermodynamik, Technische Hochschule Darmstadt, 64287 Darmstadt, Germany

(*Received* 25 *October* 1995 *and in final form* 29 *April* 1996)

Abstract—In Part I of this paper the heat and mass transfer in a pipe with a wavy surface was studied numerically. To validate the predictions and to close the gap in the Reynolds number range $400 < Re_{dm} < 2000$, where a numerical simulation of the transitional flow structure was not possible, an experimental investigation was performed. Applying the naphthalene sublimation technique, the local mass transfer was studied along the axis of the pipe. Using analogy functions, the measured Sherwood numbers were transformed into Nusselt numbers. In addition to the results of the mass transfer measurements this paper also presents flow visualization experiments. Copyright © 1996 Elsevier Science Ltd.

1. INTRODUCTION

The numerical studies of heat and mass transfer in a tube with periodically converging–diverging cross section, reported in Part I of this paper, exhibit, especially in turbulent flow, a dramatic variation of the convective wall transport in axial direction over one wavelength. To validate the predicted values an experimental technique has to be applied, which provides the required local resolution and allows the investigation of the transition from laminar to turbulent flow, which is expected to take place somewhere downstream in the pipe.

There are in existence some former studies about convective transport enhancement in tubes with axially varying cross section, e.g. Sparrow and Prata [1] applied the naphthalene sublimation technique in order to measure the convective mass transport. However, they divided the tube into single elements, each half a wavelength long, and determined the average mass flow rate and Sherwood number per half-wavelength by weighing the elements before and after sublimation. It is obvious that this method does not allow one to determine the local mass transfer coefficients which are required to validate the calculated Sherwood number distribution, especially in case of turbulent flow.

Nishimura *et al.* [2–4] applied an electro-chemical method to predict the convective mass transfer in a wavy channel. They measured the local mass transfer at eight points per wavelength in an axial direction, which again does not provide the desired resolution of the local Sherwood number distribution.

In this study, the naphthalene sublimation technique was also applied to determine the mass transfer. But, instead of measuring the averaged mass flow rate of the sublimate by a weighing procedure, the local thickness of a thin naphthalene layer, coating the inner surface of a sinusoidal pipe (1980 mm in length, with 10.5 waves), was measured at 850 points in an axial direction. From the difference in thickness before and after sublimation, the local mass transfer rates as well as the local Sherwood numbers could be evaluated. The high resolution of one measurement point every 2.3 mm guarantees a reliable basis for a comparison with the numerical predictions. The fundamentals of this measurement technique were given by Berg [5].

Another purpose of this study is to examine the onset location of transport enhancement, which is caused by the transition from laminar to turbulent flow. Transition is expected for flows with a Reynolds number $Re_{dm} > 400$, as a function of the axial coordinate.

To allow a qualitative validation of the predicted flow field the smoke visualisation technique was applied for laminar flow. Moreover the pressure loss over the complete test section was measured in order to find out whether the convective transport enhancement goes along with an increased pressure loss, as predicted in Part I.

2. EXPERIMENTS

2.1. *Mass transfer measurements*

For the determination of heat transfer coefficients and Nusselt numbers it was considered to be highly advantageous to perform mass transfer experiments in conjunction with the analogy between heat and mass transfer. The sublimation took place in the horizontally mounted experimental apparatus shown in Fig. 1. The air entered the calming section via a care-

NOMENCLATURE

A_c	cross-section
c	mean concentration
D_{12}	diffusion coefficient
d_m	mean diameter
h	amplitude of the wallfunction
m	mass rate per unit area
Nu	Nusselt number ($\alpha d_m/\lambda$)
p	pressure
Pr	Prandtl number (ν/a)
r	radial coordinate
R	individual gas constant
Re_{dm}	Reynolds number ($U_m d_m/\nu$)
Sc	Schmidt number (ν/D_{12})
Sh	Sherwood number ($\beta d_m/D_{12}$)
T	absolute temperature
t	time
u	axial velocity component
U_m	mean axial velocity
x	axial coordinate.

Greek symbols

α	heat transfer coefficient
β	mass transfer coefficient
γ_h, γ_Λ	dimensionless geometry parameters
δ	thickness of the naphthalene layer
λ_W	friction coefficient $(d_m/10\Lambda)(\Delta p/\frac{1}{2}\rho U_m^2)$
Λ	wavelength of the wallfunction
ν	kinematic viscosity
ρ	denisty
ξ	wave number
Ψ	analogy function.

Subscripts

b	bulk
corr	correction
m	average value over cross section
N	naphthalene
0	initial state, transformed coordinates
sg	saturated
W	at the wall
1/2	before/after sublimation.

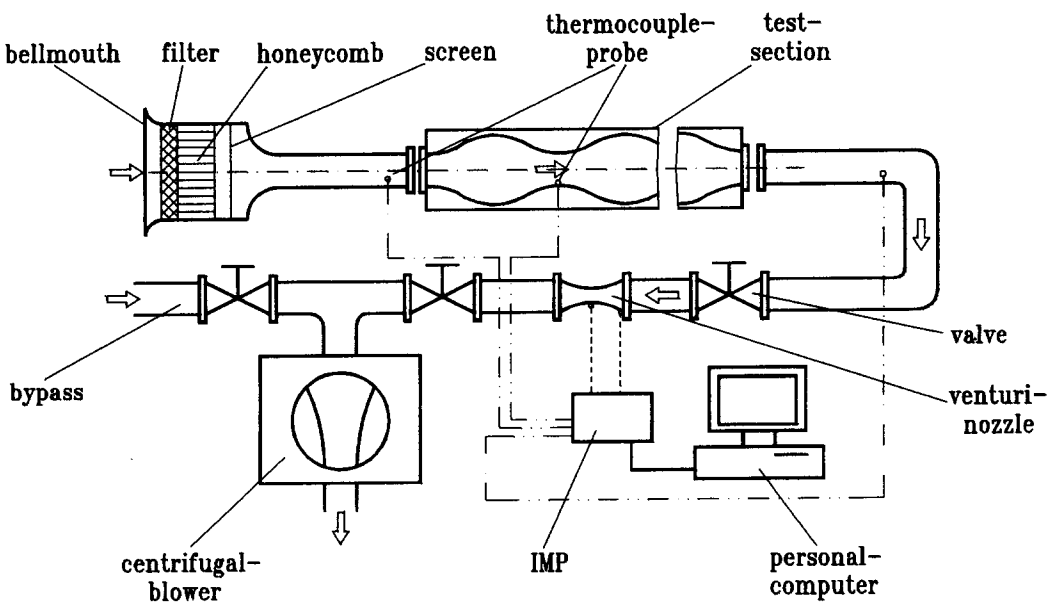

Fig. 1. Experimental apparatus.

fully styled bellmouth. The calming section consists of an air filter, a honeycomb and a wire mesh screen. After leaving the calming section the air passed through a constriction and a pipe flow development tube, before entering the test section. This was made up of 10.5 interlocking modules; each module, $\Lambda = 0.1885$ m in length and with an amplitude of the sinusoidal wall function $h = 0.01$ mm, represents one wave. With a mean diameter of $d_m = 0.06$ m the geometrical parameters are $\gamma_h = 2h/d_m = 0.333$ and $\gamma_\Lambda = 2\Lambda/d_m = 6.28$. The mass flow of the air is controlled by two valves and determined with the help of the pressure difference at a calibrated venturi nozzle. A centrifugal blower is arranged at the end of the test rig to avoid heating and flow disturbance. During a data run periodic measurements were made of the naphthalene wall temperature in every module, the flow rate and the air temperature. The temperatures

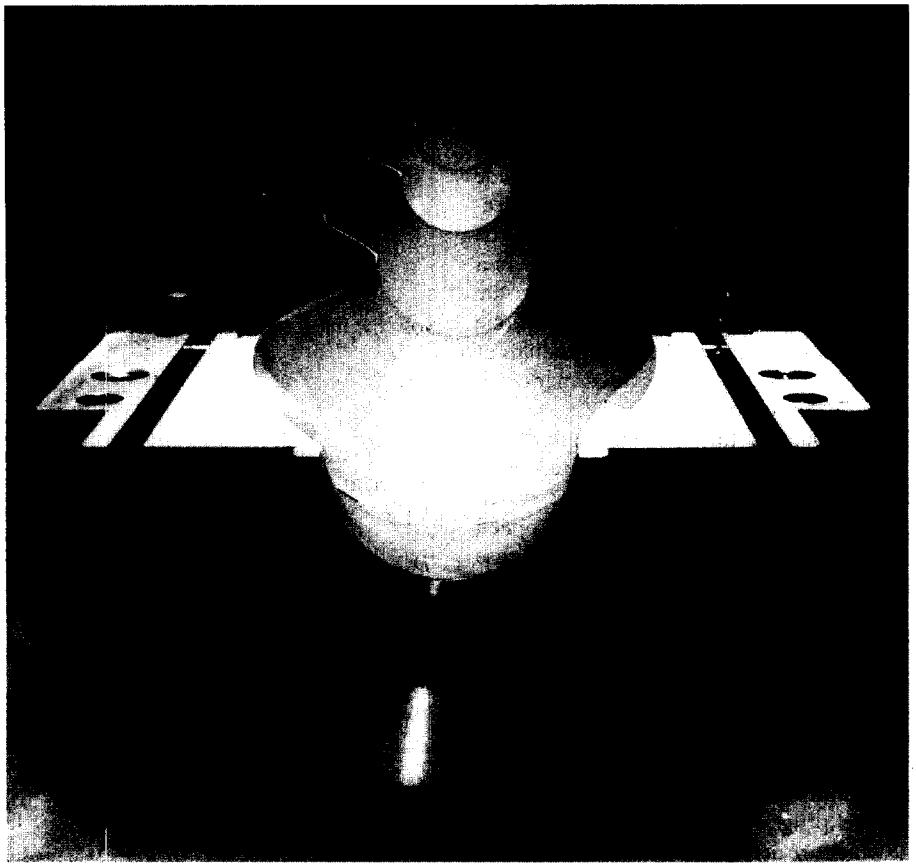

Fig. 2. Modules, coated with naphthalene.

were measured using thermocouples and the pressure difference across the venturi nozzles was measured with a pressure cell. The signals of the thermocouples and the pressure cell were registered by a data acquisition unit, which consisted of a measurement port and a personal computer with a specially developed software tool.

Each module consisted of a cuboid aluminium shell, parted in the longitudinal direction. The inner surface formed the sinusoidal wave and was coated with a $4\text{–}6 \times 10^{-4}$ m thick layer of solid naphthalene. To achieve a thin and homogeneous sublimation layer on the inner surface of the pipe, a casting device was manufactured. With the help of a vacuum pump the molten naphthalene was sucked from a melting pot into a thin gap between a heated, sinusoidally shaped kernel and the vertically arranged module. Fig. 2 shows one half of the test section, coated with the thin naphthalene layer.

To determine the thickness of the naphthalene layer, numerically controlled measurement equipment was constructed. A compound micrometer motion table allowed the exact scanning of the sinusoidal surface with an eddy-current probe. With this probe the coating thickness was measured at 81 points per module in an axial direction—the measurement error of the probe is about 10^{-6}. In order to achieve a relative measurement error of 1%, the mean thickness difference of the naphthalene layer before and after the sublimation must be 10^{-4} m. Therefore, the test runs had to last about 70 h for $Re_{dm} = 300$ and 7 h for $Re_{dm} = 13\,000$. These Reynolds numbers define the range of investigation.

The experiment started with the coating procedure of the modules, afterwards the thickness of the naphthalene layer was measured in each module. A computer controlled the micrometer motion table and recorded the thickness of the layer. Then the modules were assembled in the test rig and the blower was started. After the sublimation-run the remaining thickness of the naphthalene layer was measured.

To obtain a correction for possible extraneous sublimation that might have occurred during preparation, assembly and disassembly, a so-called 'after-run' was performed at which the whole procedure of the data run was repeated, with the exception that the blower was not activated. With the measured thickness of the naphthalene layer before and after the sublimation and the recorded temperatures of air and naphthalene during the sublimation, the calculation of the Sherwood number, which is explained in detail in Section 2.3, was performed.

2.2. *Flow visualization experiments*

An exact validation of the predicted flowfield would require the measurement of the velocities and their

turbulent fluctuations. A more superficial method to get a qualitative overview of the flow structure is the smoke visualization technique, which was applied in this study. For these experiments a glass-pipe (with the same wall shape as the aluminium modules) two waves long was fitted into the test section. The inside of the pipe was partly painted black to prevent reflections of the flash light, which was connected to the camera and allowed the illumination of the flow in a longitudinal section of the middle plane. To start the experiment, gray smoke was fed into the calming zone of the apparatus, after it entered the glass modules of the test section, the camera was triggered manually. Figure 7, which is discussed later, visualizes the flow field for $Re_{dm} = 400$. On the photograph one can clearly distinguish between the gray coloured main flow and the secondary flow in the bulge part, which remains black. This technique was successfully applied in laminar and weakly transitional flows. In the case of turbulent flows an increased diffusion did not allow any visual recognition of the secondary flow, as the complete cross section of the pipe was filled with smoke.

2.3. *Evaluation of the Sherwood and Nusselt numbers*

In order to evaluate the large number of recorded data a special computer program was developed. The algorithm of this program is now explained, giving the formulae which are necessary to calculate the Sherwood and Nusselt numbers. The local reduction of the layer thickness is gained from the thickness δ_1 before and δ_2 the thickness after the sublimation run:

$$\Delta\delta' = \delta_1 - \delta_2. \tag{1}$$

This value has to be corrected by δ_{corr} of the after-run:

$$\Delta\delta = \Delta\delta' - \Delta\delta_{corr}. \tag{2}$$

Now the local mass rate per unit area (surface) is obtained by:

$$\dot{m}_N = \frac{\rho_N \Delta\delta}{\Delta t} \tag{3}$$

where $\rho_N = 1145\ \mathrm{kg\,m^{-3}}$ is the density of naphthalene which is nearly constant at normal room temperatures. The time Δt notifies the duration of the sublimation run and varies according to the chosen Reynolds number as explained in Section 2.1.

The near wall concentration of naphthalene is calculated under the assumption of ideal gas behavior:

$$c_{NW} = \frac{p_{NW}}{R_N T_W}. \tag{4}$$

The wall temperature T_W in equation (4) is measured during the sublimation run and allows also the determination of the saturation pressure of naphthalene, applying the equation of Gil'denblat *et al.* [6]:

$$\log p_N = 31.23252 - \frac{8587.36}{T_W}; \quad [p_N] \triangleq \mathrm{Pa}. \tag{5}$$

In equation (4) the gas constant for naphthalene is $R_N = 64.84\ \mathrm{J\,kg^{-1}\,K^{-1}}$.

The bulk-concentration of naphthalene in the airflow is calculated following the standard definition:

$$c_{Nb} = \frac{\int_{A_c} u c_N \, d\bar{A}}{\int_{A_c} u \, d\bar{A}}. \tag{6}$$

Now the mass transfer coefficient can be determined:

$$\beta = \frac{\dot{m}_N}{(c_{NW} - c_{Nb})}. \tag{7}$$

With the mean diameter of the pipe and the diffusion coefficient of naphthalene in air according to Cho *et al.* [7]

$$D_{12} = 8.17708 \times 10^{-11} T_W^{1.983} \quad [D_{12}] \triangleq \mathrm{m^2\,s^{-1}} \tag{8}$$

the Sherwood number is defined to be:

$$Sh = \frac{\beta d_m}{D_{12}}. \tag{9}$$

Under the conditions of:

- isothermal wall temperatures;
- non reacting flow;
- no internal heat or mass sources;
- low near-wall concentration of naphthalene;

the analogy between heat and mass transfer holds. With the help of an analogy function:

$$\Psi = \frac{Nu}{Sh} = \frac{f(Pr)}{f(Sc)} \tag{10}$$

the Nusselt numbers can be calculated from the measured Sherwood numbers. Accounting for the special flow features in laminar, transitional and turbulent flow, three types of analogy functions were applied.

In laminar flow the correlation for the convective wall transport in hydrodynamically and thermally developing flow, given by Churchill and Ozoe [8] is used to calculate the analogy function:

$$f(Pr, Sc) = \left[1 + \left(\frac{x/(284x^*)}{\left[1 + \left(\frac{(Pr, Se)}{0.0468}\right)^{2/3}\right]^{1/2}\left[1 + \left(\frac{388}{\pi} \cdot x^*\right)^{-8/9}\right]^{3/4}}\right)^{4/3}\right]^{3/8} \times 5.357\left[1 + \left(\frac{388}{\pi} x^*\right)^{-8/9}\right]^{3/8} - 1/7$$

$$x^* = \frac{x}{d_m Re_{dm} \cdot (Pr, Sc)}. \tag{11}$$

To describe the effect of increasing turbulent motion in a transitional flow regime, the equation of Reinicke [9], which describes the convective transport

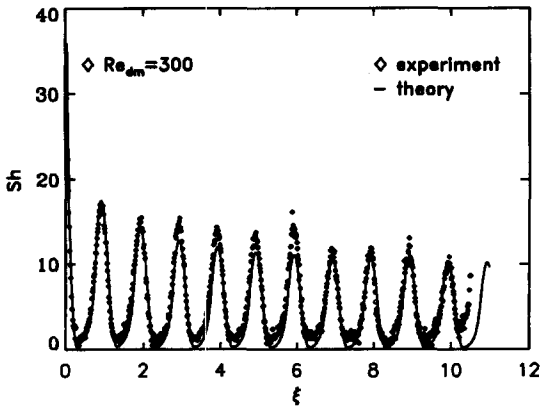

Fig. 3. Measured and predicted Sherwood number over the total length of the test section for $Re_{dm} = 300$.

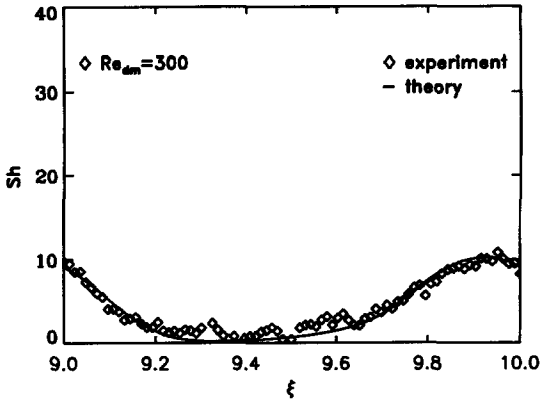

Fig. 4. Measured and predicted Sherwood number for $Re_{dm} = 300$ and fully developed flow conditions in the last wave of the test section.

in a developing boundary layer, was taken into consideration.

$$f(Pr, Sc) = \frac{0.0296 Re_x^{0.8}(Pr, Sc)}{1+1.58((Pr, Sc)-1)(Pr, Sc)^{-0.25} Re_x^{-0.1}} \tag{12}$$

with

$$Re_x = 1.25 Re_{dm} \frac{x}{d_m}. \tag{13}$$

In the entrance region of the wavy tube the flow is laminar and, therefore, equation (11) was applied. With the beginning transition, however, the analogy function equation (12) was considered to be appropriate.

For fully turbulent flow Hausen's equation for the convective transport in turbulent pipe flow [10] was utilized:

$$f(Pr, Sc) = 1.8(Pr, Sc)^{0.3} - 0.8. \tag{14}$$

With the measured pressure loss over 10 waves of the test section the wall friction coefficient becomes:

$$\lambda_W = \frac{d_m}{10\Lambda} \frac{\Delta p}{\frac{1}{2}\rho U_m^2}. \tag{15}$$

3. RESULTS AND DISCUSSION

In this section the experimentally determined Sherwood and Nusselt numbers for laminar, transitional and turbulent flow are presented in conjunction with the findings of the numerical analysis presented in Part I and supplemented by photographs of the visualization experiments. The results are plotted as a function of the wave number $\xi = x/\Lambda$.

3.1. *Laminar flow*

Figure 3 compares the measured and predicted Sherwood number for $Re_{dm} = 300$ over the total length of the test section. The agreement between the experimental findings and the numerical analysis is

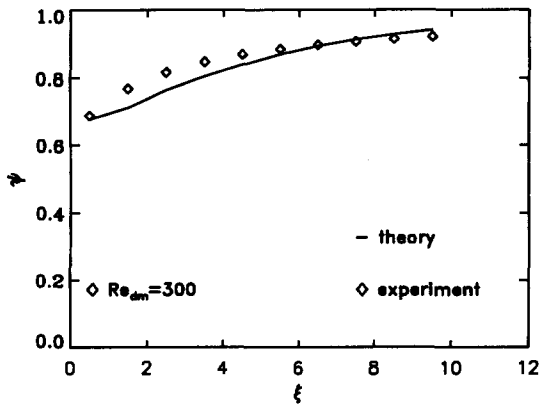

Fig. 5. Averaged values per wavelength of the analogy function for $Re_{dm} = 300$.

good, which is further confirmed by a detailed study of one wave at the end of the test section for fully developed flow conditions (Fig. 4). As outlined in Part I of this paper, the minimum in the Sherwood number is caused by the closed recirculation bubble.

Since the analogy between heat and mass transfer is frequently applied to calculate heat transfer coefficients from mass transfer experiments, the effects of flow separation and reattachment on the analogy, which go along with the recirculating bubble in the bulge part of the pipe, will be studied in detail. Another reason for this detailed study is to check the reliability of the analogy function in the range of Reynolds numbers where numerical predictions have not yet been feasible. One has to bear in mind that the determination of the Nusselt number is based on analogy functions, introduced in Section 2.3, which have been derived for merely similar flow conditions.

In Fig. 5 the mean value of the analogy function per wavelength for $Re_{dm} = 300$, calculated with the numerical algorithm, is compared with the values given by equation (11). Except for the entrance region, where the numerical analysis shows a slower development of the boundary-layer compared to the values based on the correlation, the agreement is good. The

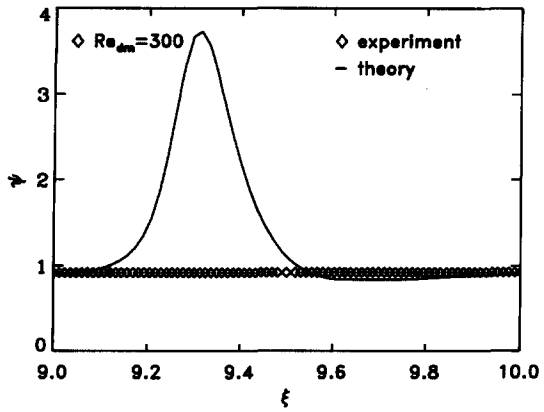

Fig. 6. Local distribution of the analogy functions for fully developed flow conditions in the last wave of the test section.

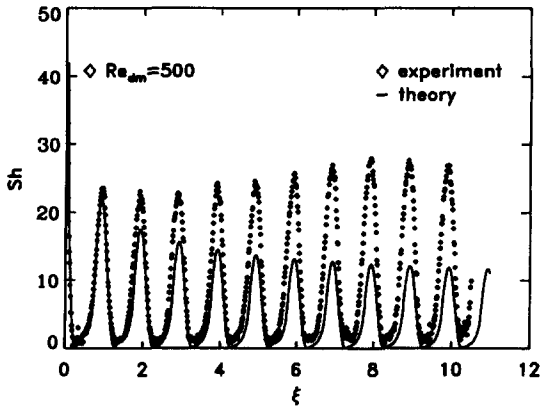

Fig. 8. Measured Sherwood number for $Re_{dm} = 500$ over the total length of the test section (transitional flow).

comparison of the local values Ψ for fully developed flow conditions in the last wave, depicted in Fig. 6, however, shows a dramatic deviation around the separation point. It is obvious that the calculated value exceeds the level of the experimental one nearly four times, clearly indicating that the transport around the separation point is diffusion dominated as discussed in Part I of this paper. The Nusselt number, therefore, is larger than the Sherwood number, which is not the case for attached flow. This phenomenon cannot be described by the analogy function equation (11) since this function is derived for convectively dominated heat and mass transfer.

Figure 7 compared the visualized flow field with the predicted streamlines for $Re_{dm} = 400$ and confirms the good agreement between measurement and predictions. Since the diffusion of smoke into the separation bubble is restrained by the shear layer, the bubble remains black on the photograph, whereas the main flow is coloured gray by the smoke.

3.2. *Transitional flow*

With increasing Reynolds number the flow pattern changes from laminar to turbulent. First indications can be observed for $Re_{dm} = 400$, for $Re_{dm} = 500$, however, they are stronger, which can be discussed by means of Fig. 8, where the measured Sherwood numbers are plotted over the complete length of the test section. At the end of the 4th wave the Sherwood number stops its exponential decay, which was already observed for $Re_{dm} = 300$ in Fig. 3, and increases again, reaching an asymptotic level at the end of the pipe. The increase is caused by the onset of three-dimensional unsteady but periodic motions of the former laminar flow. In Fig. 9 the regular laminar flow field in the 4th wave was calculated numerically and compared with the results of the flow visualization experiments. Since the numerical algorithm was developed to model stationary laminar or turbulent flow, the prediction of the flow field and Sherwood numbers behind the 4th wave is not possible.

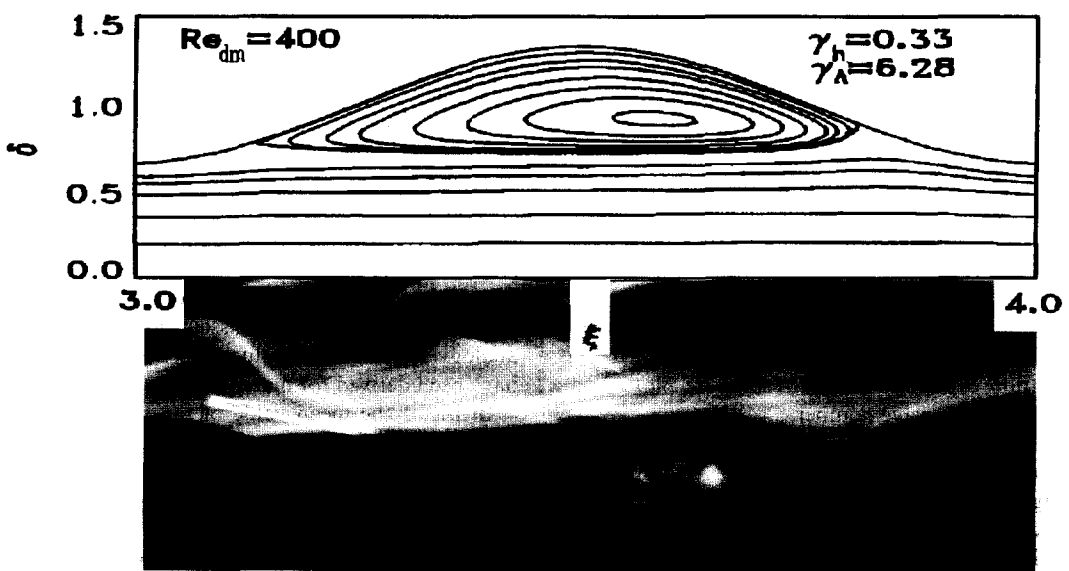

Fig. 7. Visualized and predicted flow field for $Re_{dm} = 400$.

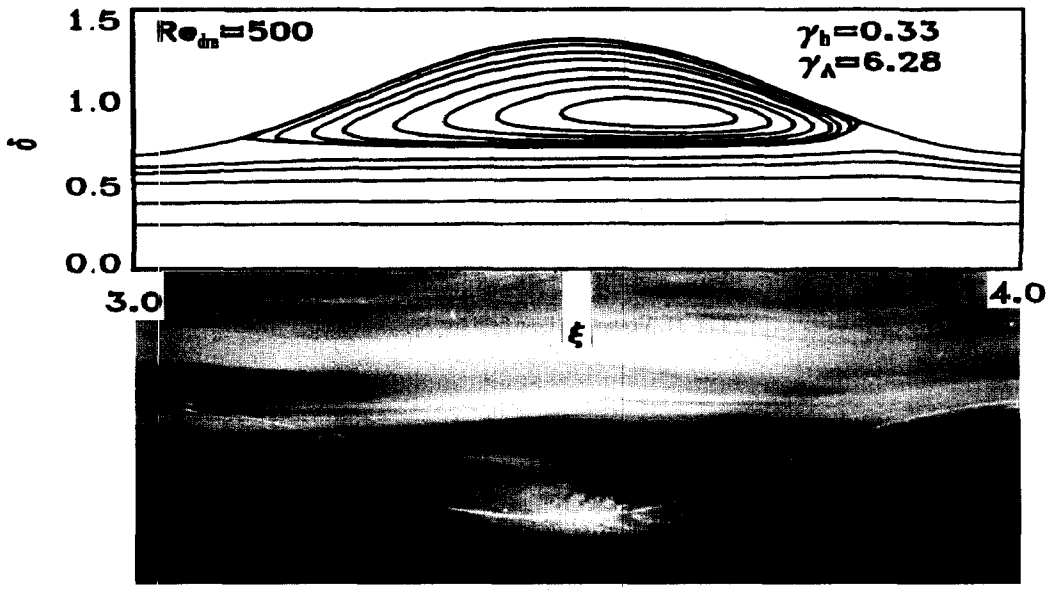

Fig. 9. Visualized and predicted flow field for $Re_{dm} = 500$.

In order to understand the transition from laminar flow to unsteady but regular transitional flow and finally to turbulent flow, the results of the visualization experiments will be discussed. For $Re_{dm} = 800$ Fig. 10 shows the photograph of the flow field, with the flow direction from left to right. This photograph evidences a nascent vortex in the shear layer at the end of the separating bubble, it is not yet clear whether this vortex will decay downstream of the reattachment point, or will be strengthened along its way through the pipe. The raise of this vortex in the shear layer is discussed in detail by Lesieur [11] and has its analogon in plane flow which is known as Kelvin–Helmholtz instability. Increasing the Reynolds numbers to $Re_{dm} = 1000$ shows clearly that now the disturbances in the shear layer can grow, leading to a timed periodic break down of the recirculation bubble (Fig. 11).

The instability process of the shear layers for $Re_{dm} > 300$ can be described by the inviscid theory, which means that the shear layer is always unstable and the growing rate of a disturbance depends on its wave number and the thickness of the shear layer, which is a function of the Reynolds number. If an initial disturbance has grown, due to the amplification process of the shear layer, and reaches a certain level after a reasonable length downstream from the entrance, it is strong enough to affect the main flow in the core region of the pipe. The level of the disturbance

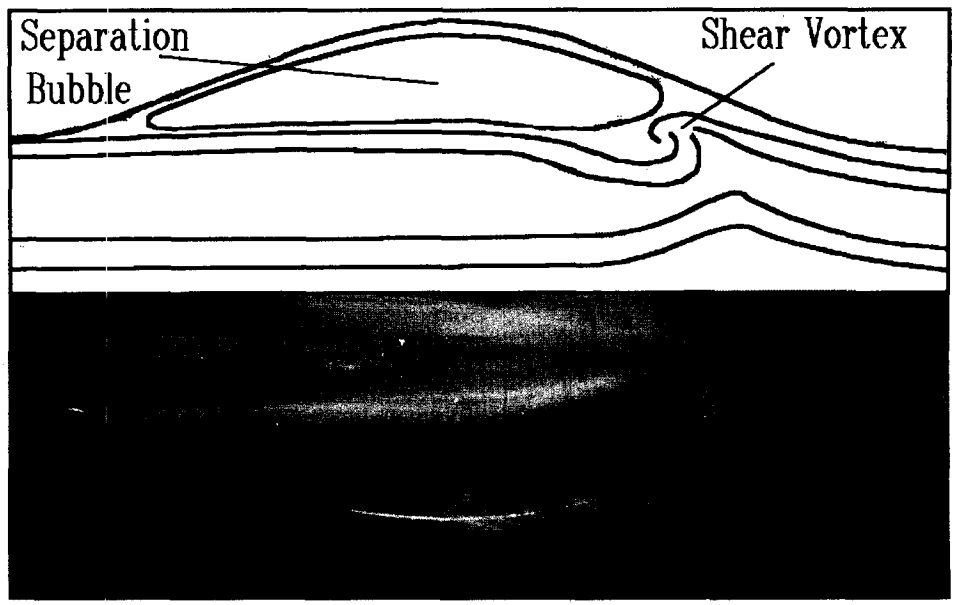

Fig. 10. Visualized flow field for $Re_{dm} = 800$.

Fig. 11. Visualized flow field for $Re_{dm} = 1000$.

which is necessary to cause the transition from laminar to turbulent behaviour of the main flow is a function of the Reynolds number and the wave number of the disturbance. Following the theory of Ghaddar *et al.* [12–13], the most critical disturbance in this complex interaction of the unstable shear layers and the main-flow in the core region of the pipe has a wave number, which is an integer of the wave number of the periodic wall function.

Fig. 12 shows the measured Sherwood number in the test section for $Re_{dm} = 2000$, clearly depicting the transition from laminar to turbulent flow behind the fourth wave, which is accompanied by a sudden increase of the wall transport. As mentioned in Part I of this paper, the numerical algorithm is not able to predict the transition itself. Therefore, Figs 13 and 14 compare the measured and predicted Sherwood numbers for $Re_{dm} = 2000$ for laminar flow in the first wave and the weakly turbulent flow in the last wave. The results show a reasonable agreement. In turbulent flow, however, near the separation point, the numerical algorithm seems to fail which may be an effect of the time independent formulation of the algorithm, since in reality the flow in this area is expected to be highly unstable.

To deduce the Nusselt number from the measured Sherwood number, the analogy function given for laminar flow by equation (11) was used in the first

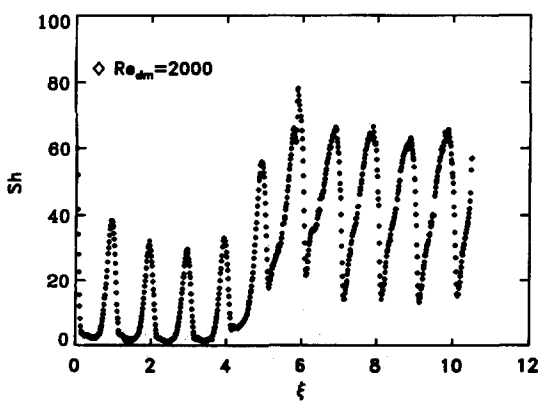

Fig. 12. Measured Sherwood number for $Re_{dm} = 2000$ over the total length of the test section (transitional flow).

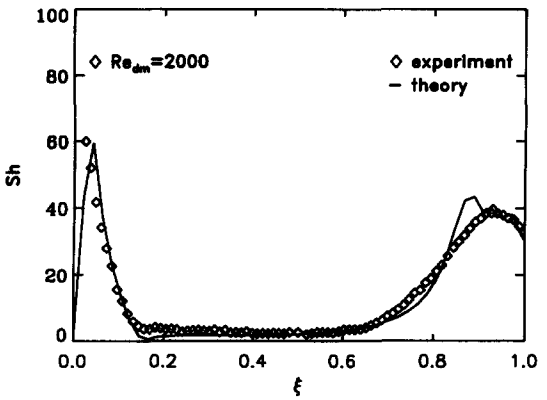

Fig. 13. Measured and predicted Sherwood number for $Re_{dm} = 2000$ in the first wave.

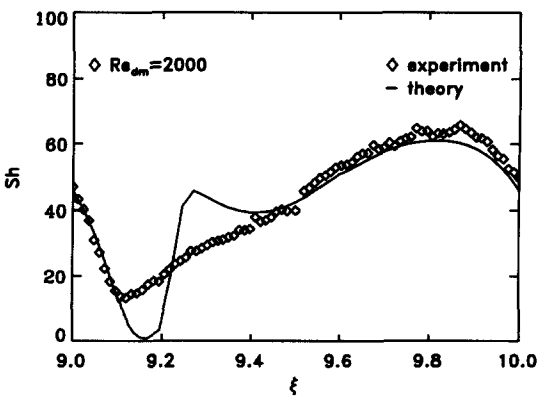

Fig. 14. Measured and predicted Sherwood number for $Re_{dm} = 2000$ in the last wave.

four waves, for the fifth wave the analogy function given in equation (12) for transitional flow was applied. The comparison of the numerically predicted analogy function with the analogy function used in the experiments shows that both functions line up well for turbulent flow at the end of the test section, as elucidated by Fig. 15. The analogy function used in the experiments shows a smooth transition from laminar to turbulent flow, modeling the increasing turbulence, whereas the prediction just switches from laminar to turbulent flow. With increasing Reynolds

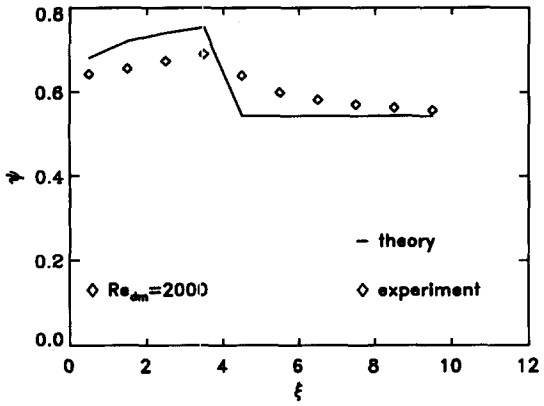

Fig. 15. Averaged values per wavelength of the analogy function for $Re_{dm} = 2000$.

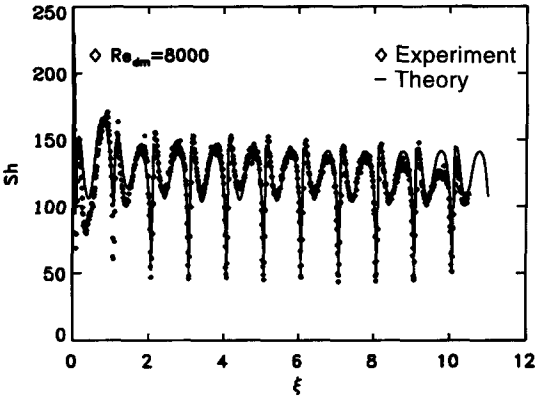

Fig. 17. Measured and predicted Sherwood number for $Re_{dm} = 7000$ over the total length of the test section (turbulent flow).

number the transition point from laminar to turbulent flow is shifted further upstream, as shown in Fig. 16 for $Re_{dm} = 7000$.

3.3. *Turbulent flow*

Figure 16 elucidates that up to $Re_{dm} = 7000$ laminar flow enters the test section, in the case of a highly calmed flow, but changes immediately to turbulent flow after the first wave. For $Re_{dm} > 7000$ no laminar flow has been observed in the test section. Figure 17 shows a good agreement between the measured and predicted Sherwood numbers for $Re_{dm} = 8000$. There are differences between measurement and predictions only in the first two waves which are mainly caused by differences of the turbulence intensity in the entrance of the test-section, compared to the fully developed velocity profile which was used for the calculations. It is assumed that the observed deviations may be due to a less turbulent flow entering the test-section and slower development to fully turbulent flow structure compared to the calculations. The detailed discussion of the flow and the turbulence field in Part I of this paper has shown that the sharp minimum–maximum sequence of the Sherwood number distribution, in the diverging part of the wave, is caused by the separation of the flow and a following layer of increased vorticety close to the wall in the developing recirculation area. The smoke technique is not able to visualize this behavior, since, in turbulent flow the smoke diffusion is very intensive, not allowing an identification of secondary flows. The point of separation, indicated by the sharp minimum in the diverging part and the reattachment point in the converging part of the wave, elucidated by the second maximum, are well predicted.

Figure 18 shows the comparison of the predicted local analogy function and the distribution calculated by the analogy function given in equation (13). The comparison again exhibits that, as observed for laminar flow, deviations occur near the separation and reattachment point, induced by variations of the concentration boundary layer which cannot be predicted by analogy functions. The mean values per wavelength show a better agreement.

4. CONCLUSIONS

The experimental investigation of mass transfer in a pipe with a sinusoidal varying diameter yields a good agreement with the numerically predicted values presented in Part I of this paper. It was possible to

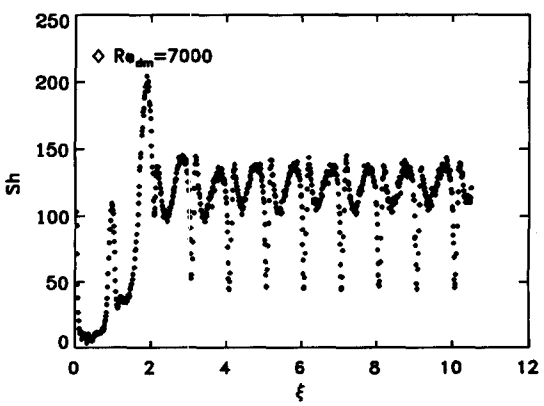

Fig. 16. Measured Sherwood number for $Re_{dm} = 7000$ over the total length of the test section.

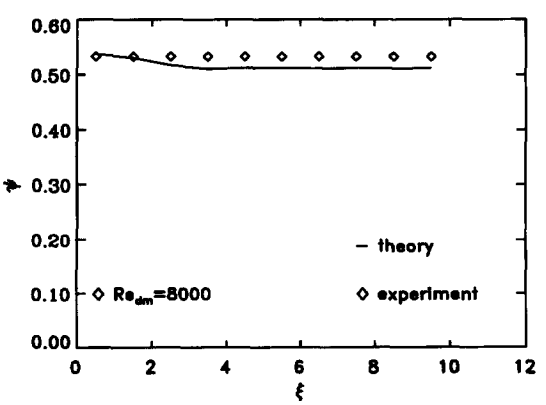

Fig. 18. Averaged values per wavelength of the analogy function of $Re_{dm} = 8000$.

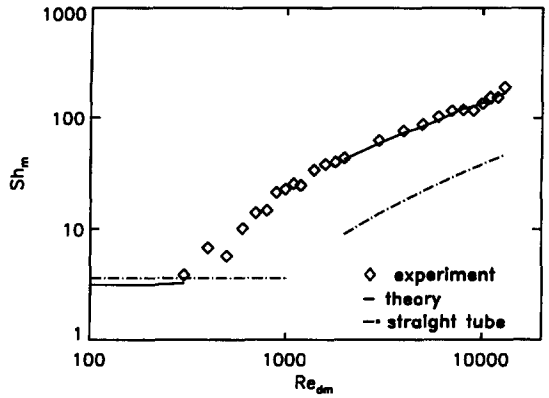

Fig. 19. Averaged values per wavelength of the Sherwood number for fully developed flow conditions.

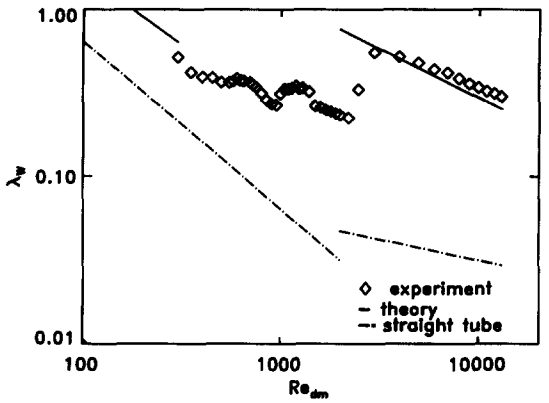

Fig. 21. Friction coefficient as a function of the Reynolds number.

close the gap of the transitional flow regime ($400 < Re_{dm} < 2000$) which had to remain unsolved by the numerical analysis. In this case the measured Sherwood numbers reveal a sudden increase after a distinct length of laminar flow in the entrance part of the test section.

In Fig. 19 the mean Sherwood numbers (wave-averaged for fully developed flow conditions) are plotted as a function of the Reynolds number. For laminar flow the Sherwood numbers are lower than those obtained for a straight pipe because the recirculating bubbles impede mass transfer. In the case of laminar and turbulent flow the numerically predicted values coincide quite well with the experimental results.

The use of analogy functions, based on heat transfer correlations for the flow through a straight pipe has proven to be a useful tool in calculating Nusselt numbers from measured Sherwood numbers. The results are summarized in Fig. 20 which depicts the mean Nusselt numbers as a function of the Reynolds number. A detailed analysis of the local distribution has shown uncertainties in areas where the heat and mass transport is diffusion dominated, e.g. near the separation point.

The flow visualization experiments, applying the smoke technique, show a good agreement with the predictions and show that the instability process, which leads to transitional flow, is similar to that known as Kelvin–Helmholtz instability for plane shear flow. As predicted in Part I of this paper, the increase of the convective transport is accompanied by an increased friction coefficient which is depicted in Fig. 21.

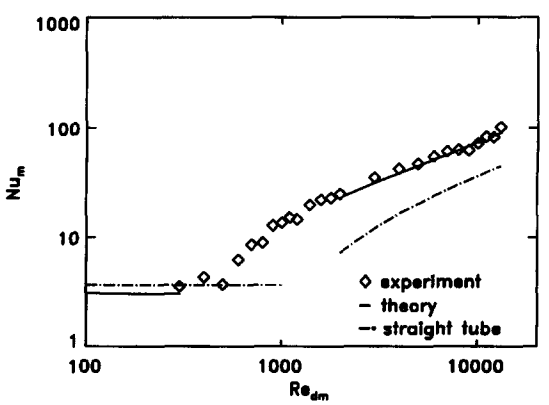

Fig. 20. Averaged values per wavelength of the Nusselt number for fully developed flow conditions.

REFERENCES

1. E. M. Sparrow and A. T. Prata, Numerical solution for laminar flow and heat transfer in a periodically tube converging–diverging, with experimental confirmation. *Numerical Heat Transfer*, 1983, **6**, 441–461.
2. T. Nishimura, Y. Ohori and Y. Kawamura, Flow characteristics in a channel with symmetric wavy wall for steady flow. *Journal of Chemical Engineering of Japan*, 1984, **17**, 466–471.
3. T. Nishimura, Y. Ohori, Y. Kajimoto and Y. Kawamura, Mass transfer characteristics in a channel with symmetric wavy wall for steady flow. *Journal of Chemical Engineering of Japan*, 1985, **18**, 550–555.
4. T. Nishimura, Y. Kajimoto and Y. Kawamura, Mass transfer enhancement in channels with a wavy wall. *Journal of Chemical Engineering of Japan*, 1986, **19**, 142–144.
5. P. Berg, Experimentelle Bestimmung des örtlichen Wärmeübergangs von Turbinen Leit- und Laufschaufeln mit Hilfe der Analogie zwischen Wärme- und Stoffübergang. Ph. D. thesis, Technische Hochschule Darmstadt, Darmstadt, 1991.
6. I. A. Gil'denblat, A. S. Furmanov and N. M. Zhavoronkov, Vapor pressure over crystalline naphthaline. *Journal of Applied Chemistry*, 1960, **33**, 246.
7. K. Cho, T. F. Irvine and J. Karni, Measurement of the diffusion coefficient of naphtalene into air. *International Journal of Heat & Mass Transfer*, 1992, **35**, 957–966.
8. S. W. Churchill and H. Ozoe, Correlations for laminar forced convection in flow over an isothermal flat plate and in developing and fully developed flow in an isothermal tube. *Journal of Heat Transfer*, 1973, **95**, 416–419.
9. H. Reinicke, Über den Wärmeübergang von kurzen durchströmten Rohren und querangeströmten Zylindern verschiedener Anordnung an zähe Flüssigkeiten verschiedener Prandtl-Zahl bei kleinen Temperaturdifferenzen. Ph.D. thesis, Technische Hochschule Darmstadt, Darmstadt, 1969.
10. H. Hausen, Erweiterte Gleichung für den Wärme-

übergang in Rohren bei turbulenter Strömung. *Wärme- und Stoffübergang*, 1974, **7**, 222–225.
11. M. Lesieur, *Turbulence in Fluids*, 2nd edn. Kluwer Academic, Dordrecht, 1990.
12. N. K. Ghaddar, K. Z. Korczak, B. B. Mikic and A. T. Patera, Numerical investigation of incompressible flow in grooved channels, Part I stability and selfsustained oscillations. *Journal of Fluid Mechanics*, 1986, **163**, 99–127.
13. N. K. Ghaddar, K. Z. Korczak, B. B. Mikic and A. T. Patera, Numerical investigation of incompressible flow in grooved channels, Part II resonance and oscillatory heat transfer enhancement. *Journal of Fluid Mechanics*, 1986, **168**, 541–567.